Modeling of Armour-piercing Projectile Perforation of Thick Aluminium Plates

Kasper Cramon Jørgensen, Vivian Swan
NIRAS A/S, Sortemosevej 19, DK-3450 Allerød

Abstract

This study investigates the perforation process of armour-piercing projectiles on commercially available high-strength aluminium. A LS-DYNA® model is developed with thick target plates of aluminium alloy 7075-T651 and an incoming 7.62 mm armour-piercing projectile with an impact velocity of 850 m/s. A numerical formulation combining classic Lagrangian finite elements with an adaptive mesh algorithm is utilized to overcome large deformation challenges and more accurately predict failure mechanisms.

Both aluminium target and projectile have been modelled as deformable with a modified version of the Johnson-Cook strain-rate and temperature dependent plasticity model, based on input parameters from literature. Main model results include projectile residual velocity after target perforation and prediction of target failure mechanism. The model results are validated against experimental results from live ballistic tests and a sensitivity study is carried out to identify influential material model parameters.

Keywords: ballistic impact, high-strength aluminium, modified Johnson-Cook, adaptive mesh, failure mechanism

Introduction

Ballistic tests (or firing tests) are used to assess the protective capability of a ballistic armour plate. The main result of such a ballistic test is the velocity drop of the projectile in the ballistic plate.

In addition to ballistic tests, computer simulations such as finite element analyses can be carried out. In a computer simulation the actual test setup from a ballistic test can be replicated and the predicted projectile velocity drop can then be validated against the ballistic test. A validated computer simulation offers, in addition to a velocity drop prediction, a prediction of the failure mechanism which is a result that is not immediately available in the ballistic test.

In this study a LS-DYNA model is developed that simulates a 7.62 mm armour-piercing projectile perforating a thick target plate of aluminium alloy 7075-T651. The specific aluminium alloy is chosen because it is thoroughly described and investigated in papers relating to ballistic behaviour and performance. The model setup is based on the work by Børvik et al. with a Lagrangian finite element formulation with a continuously adaptive mesh.

LS-DYNA Model

A LS-DYNA finite element model is developed which simulates a projectile that perforates an aluminium target. The LS-DYNA SMP LS-DYNA R6.1.1 solver is used. An initial velocity condition of 850 m/s is given to the projectile with *INITIAL_VELOCITY_GENERATION and

the interaction between projectile and target is modelled with an automated frictionless contact (*CONTACT_2D_AUTOMATIC_SINGLE_SURFACE).

Shell element formulation 15 corresponding to the volume weighted 2-D axisymmetric solid element is used for both target and projectile. In an axisymmetric setup, the rotational symmetry of the projectile is utilized as shown in Figure 1. This also means that the target plate is assumed circular with a radius of 150 mm and that the projectile impacts the exact midpoint of the circular plate.

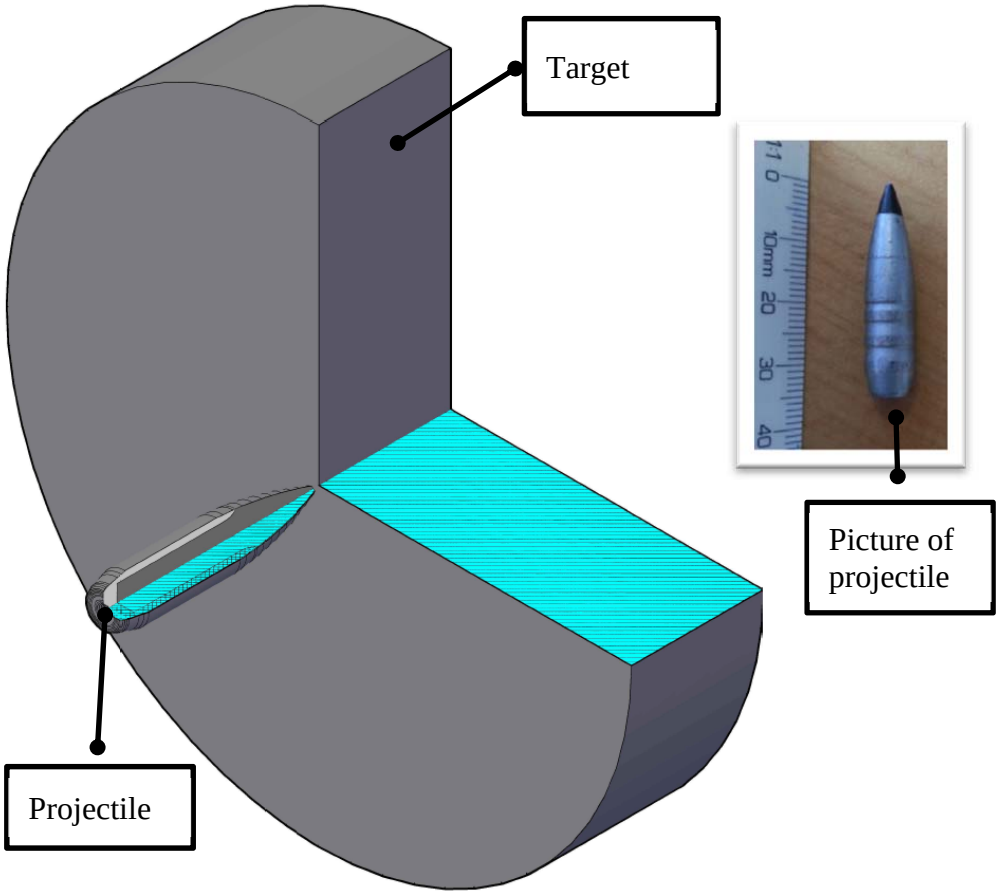

Figure 1. 2-D axisymmetric model setup where rotational symmetry is utilized to give a 3-D behaviour with a much simpler 2-D model. The hatched cyan cross-section is the 2-D area that is modelled geometrically.

Target

The ballistic performance of thick plates of the high strength aluminium alloy 7075-T651 is investigated.

Two targets with thicknesses 20 mm and 28 mm are modelled. A target material model with data from [2],[4],[6] is used in the present study, see Table 1.

Projectile

A 7.62 mm armour-piercing projectile is used to investigate the ballistic performance of the aluminium plate. Due to confidentiality further projectile specification is not given. The projectile has a total mass of 9.57 grams and consists of a hardened steel core that sits in a brass-

shoe. A high precision geometric model of the projectile is established in two steps. In the first step, the projectile surface is established with a 3-D scan. In the second step, the projectile is filed down and the internal boundary between the shoe and core is established by simple measurement techniques.

Indentation hardness tests have been carried out on the two metals of the sanded down projectile. The core and shoe hardness is close to that of equivalent tests performed on a 7.62 mm AP projectile in [1]. The projectile material models proposed in [1] are therefore also used in the present study, see Table 1.

Mesh

The model geometry with a close up on the finite element mesh is shown in Figure 2. An element side length of 1/8 mm is used in the model based on an element size sensitivity study which is described later in this paper.

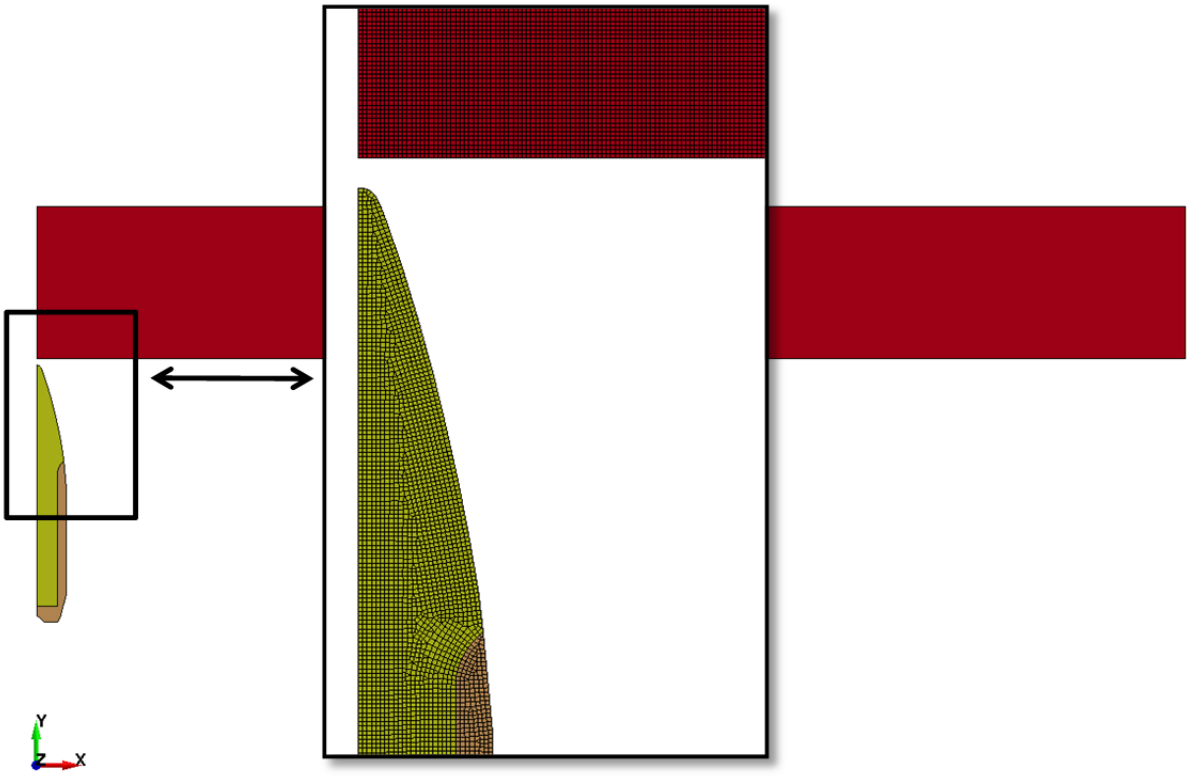

Figure 2. 2-D geometry of finite element model with aluminium target (red area), projectile steel core (yellow area) and projectile brass-shoe (brown area). Also a close up on the finite element mesh.

With *CONTROL_ADAPTIVE card, adaptive meshing is activated on the target mesh to overcome large deformation challenges. It is not necessary to activate adaption of the projectile mesh as the projectile deformation is relatively small.

For 2-D axisymmetric problems an r-adaptive algorithm is available in LS-DYNA. In this algorithm, a completely new mesh is generated for every adaption which includes a renumbering of nodes and elements. The advantage of the adaptive mesh is that severely distorted elements are avoided. This is illustrated in Figure 3 where a mesh without adaption is compared with an

adaptive mesh. Fringe levels show the element aspect ratio which is the proportion between the side lengths of an element, with unity (1) being the perfect finite element.

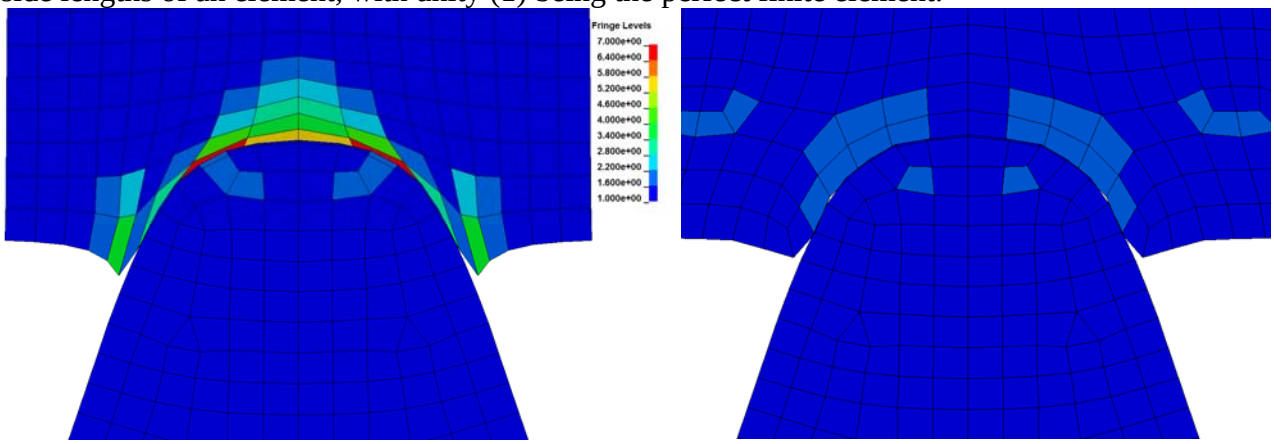

Figure 3. Projectile entering target plate with fringe levels of the aspect ratio. For the same snapshot in time two different model outputs are shown: Mesh without adaption (left) and mesh with adaption (right). The fringe levels show an aspect ratio of up to 7 without adaption and below 2 with adaption.

A significant disadvantage with this axisymmetric adaptive mesh algorithm is that all elements adapt to the same size and that a part with adaptive mesh cannot be attached to another part. This means that all elements in the target mesh have the same size even though equally accurate results could be obtained by applying a mesh with biased node spacing and with the smallest elements near the projectile impact zone.

The time interval between mesh adaptions is specified with the adaption-frequency variable ADPFREQ. With an appropriate choice of adaption frequency the aspect ratio is kept reasonably low and the time step reasonably high. Note that the algorithm struggles when element erosion (i.e. when elements are removed) is introduced. This however can for the most part be avoided with an appropriate choice of adaption frequency combined with the inclusion of material splitting with *PART_ADAPTIVE_FAILURE. With material splitting the adaptive-mesh part is split in two when the thickness reaches a specified minimum, which in the present study is set to 0.1 mm.

The choice of adaption frequency is a trade-off between simulation time and accuracy since increasing the frequency dramatically increases simulation time and reducing the frequency gives poorer aspect ratios in between mesh updates. Based on trial and error an adaption frequency of 5e-4 msec was found appropriate with an increased frequency of 2e-4 msec around the time the projectile nose reaches the backside of the plate.

Material Models

The aluminium target (Al7075-T651), the projectile hardened steel core and the brass-shoe are all modelled with the modified Johnson-Cook model (MJC). In MJC the equivalent flow stress (Von Mises stress) is modelled as:

$$\sigma_{eq} = \left(A + B\varepsilon_{eq}^{n}\right)\left(1 + \dot{\varepsilon}_{eq}^{*}\right)^{C}\left(1 - T^{*m}\right) \qquad \text{Eq. 1}$$

where A, B, C, n and m are material parameters. ε_{eq} is the equivalent plastic strain and $\dot{\varepsilon}^{*} = \dot{\varepsilon}_{\mathrm{p}}/\dot{\varepsilon}_{0}$ is the normalized equivalent plastic strain-rate where $\dot{\varepsilon}_{0}$ is the strain rate used in quasi-static tensile tests. T^{*} is the homologous temperature which corresponds to a ratio between the current temperature and the melting temperature.

Failure is modelled with the Cockcroft and Latham (CL) criterion, where an element is eroded when $D = 1$:

$$D = \frac{1}{W_{cr}} \int_0^{\varepsilon_{eq}} max(\sigma_1, 0)\, d\varepsilon_{eq} \qquad \text{Eq. 2}$$

σ_1 is the maximum principal stress and W_{cr} is the total plastic work when failure is reached. An additional failure criterion is included stating that an element is eroded when the temperature reaches a critical value.

The MJC is available in LS-DYNA with material type 107: *MAT_MODIFIED_JOHNSON_COOK. Comparing with LS-DYNA material type 15 which is the very popular standard Johnson-Cook model (JC) the most notable differences are in the strain rate dependence term and the failure criterion [7]. Especially the CL criterion is far simpler than the JC failure criterion. Furthermore, in contrast to JC, MJC does not require an equation of state and no spall failure model is available.

The material model parameters are listed in Table 1 below.

Parameter	**Unit**	**Modified Johnson Cook *MAT_107**			**Johnson-Cook *MAT_15**
		Target Al7075-T651	**Projectile**		
			Steel	**Brass**	**Target Al7075-T651**
Young's modulus E	GPa	71.7	210	115	71.7
Shear modulus G	GPa	-	-	-	26.9
Poisson's ratio ν		0.33	0.33	0.31	0.33
Density ρ	$\frac{\text{kg}}{\text{m}^3}$	2810	7850	9059	2810
Yield strength A	MPa	520	1200	206	520
Strain hardening parameter B	MPa	477	50000	505	477
Strain hardening parameter n		0.52	1	0.42	0.52
Strain rate in static tensile tests $\dot{\varepsilon}_0$	$1/s$	5e-4	5e-4	5e-4	5e-4
Modified strain rate sensitivity const. C		0.001	0	0.01	-
Strain rate sensitivity constant C_{JC}		-	-	-	0.0025
Reference temperature	K	293	293	293	293
Melting temperature	K	893	1800	1189	893
Critical temperature parameter, T_c	K	804	1620	1070	-
Thermal softening parameter m		1.61	1	1.68	1.61
Specific heat capacity with respect to mass, C_p	$\frac{\text{J}}{\text{kg} \cdot \text{K}}$	910	452	385	910
Taylor-Quinney coefficient, χ		0.9	0.9	0.9	-
Thermal expansion coefficient, α	$1/\text{K}$	2.3e-5	1.2e-5	1.9e-5	-
Critical Cockcroft-Latham const. W_{cr}	MPa	106	Inactive	Inactive	-
Johnson-Cook failure model		-	-	-	D_1=0.096, D_2=0.049 D_3 =3.465, D_4=0.016 D_5=1.099
*EOS_GRUNEISEN	-	-	-	-	C_0=5240 $\frac{\text{m}}{s}$, S_1=1.4, V_0=1 S_2=S_3=a=E_0=0, Γ_0=1.97

Table 1. Material model parameters for the target and projectile metals [1],[2],[3],[4],[6],[8]. The brass density is adjusted to ensure correct kinetic energy of projectile. The standard Johnson-Cook model is used only in a sensitivity study.

Model Results and Test Comparison

Live ballistic tests were carried out. For each plate thickness, measurements of initial and residual projectile velocity were obtained for six successful tests. A comparison of modelled and measured velocity is listed in Table 2. Due to confidentiality the residual velocity is normalized according to the residual velocity predicted by the model.

Target plate thickness	Normalized residual velocity	
	Numerical model	Ballistic test (std. dev.)
20 mm	1	5% from numerical model (4-6%)
28 mm	1	12% from numerical model (7-17%)

Table 2. Model results compared with live tests for 7.62 mm AP projectile vs. Al7075-T651 target.

The standard deviation of the ballistic tests on the 28 mm plate clearly shows a large discrepancy in the residual velocity of the projectile. In general it should be noted, that the test measurements have a rather large uncertainty and therefore it cannot be concluded that the ballistic test result is a truly accurate result and that the model prediction is off by 5-12%.

Snapshots of the projectile perforating the target plate with fringe levels of the cumulative damage parameter D in the target material are displayed in Figure 4. Failure is introduced in a finite element by element erosion when D cumulates to one.

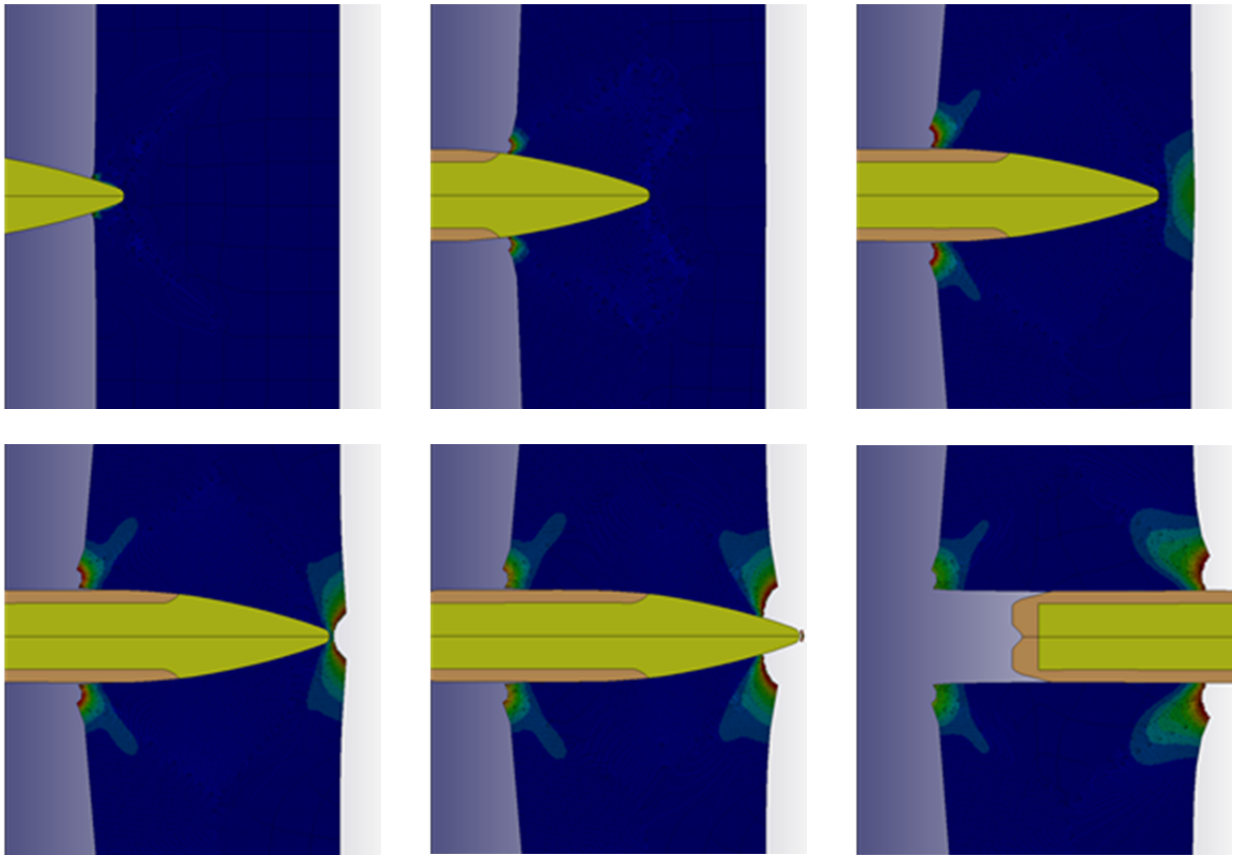

Figure 4. Snapshots of projectile perforation of the target. Fringe levels of the material model damage parameter *D* are shown in target.

The failure mechanism as predicted by the model can be established from the sequence of snapshots in Figure 4. In the penetration process, target material expands over the projectile and the aluminium is pushed aside to leave room for the projectile. The projectile fully perforates the target and a hole in the trajectory of the projectile is left in the target. A broad compression zone is generated with considerable compressive plastic strains in the target. In addition, out-of-plane tensile deformation is observed in the front and backside of the target, with following element erosion due to tensile failure. This failure mechanism is known as ductile hole enlargement and from visual inspection this also seems to be the failure mechanism seen in live ballistic tests.

It is interesting to observe that elements are mainly eroded in the zones of out-of-plane tensile deformation. This agrees well with the CL criterion where only tensile failure is possible. Additional elements are eroded because the temperature reaches a predefined critical value. This however, only happens immediately in front of the projectile nose and the number of elements that meets this criterion is very small compared to the number of elements failing due to the CL criterion. Erosion due to elements reaching the critical temperature criterion is therefore most likely negligible relative to the overall failure mechanism and projectile velocity reduction. Extrapolating on this result, it is likely that when modelling projectile perforation of thick targets with ductile hole-enlargement failure-mechanisms, the failure model has minor influence on the residual velocity of the projectile.

Small spall flakes on the backside of the target plate are observed in live ballistic tests (see Figure 5) which are not predicted by the numerical model. Spall failures can be modelled with JC, but with MJC a spall failure model is not available. That said, the small spall flakes seems to be of minor importance in relation to failure mechanism and especially in relation to the residual velocity of projectile.

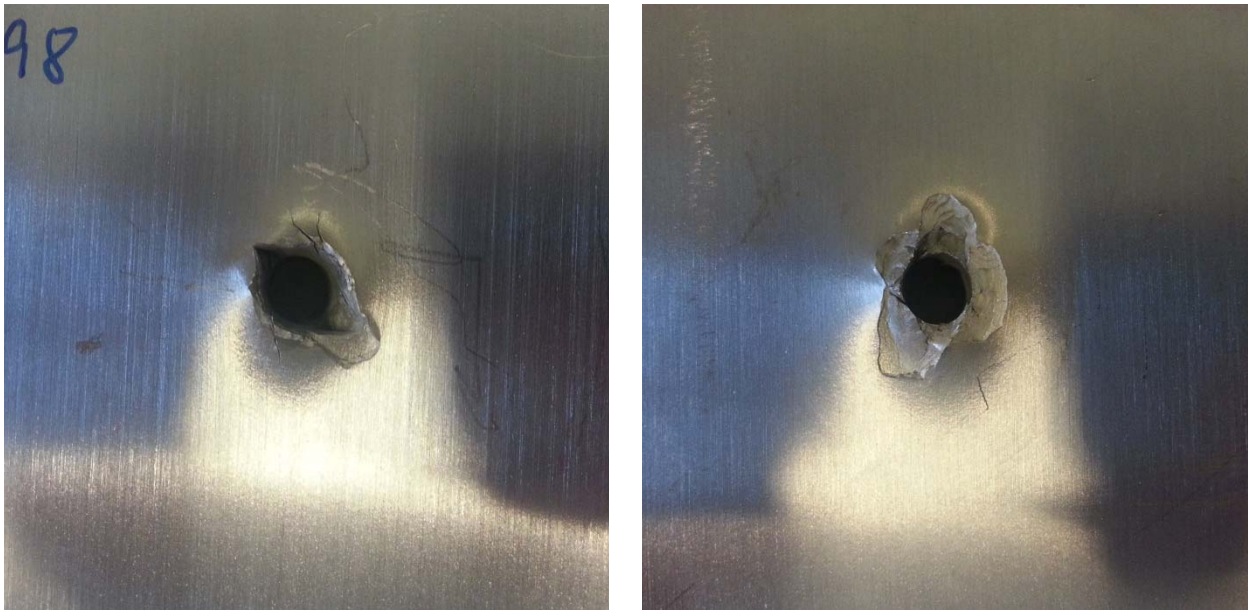

Figure 5. Hole from 7.62 mm armour-piercing projectile in 20 mm thick target plate. Left: front side of plate where projectile enters. Right: Back side of plate where projectile leaves.

The maximum equivalent plastic strain observed in the projectile is approximately 2%, with the largest deformations in the front of the hardened steel core and in the front of the brass shoe

(Figure 6). From an energy balance it is seen that almost all the kinetic energy taken out of the projectile is converted to internal energy in the target i.e. deformation of target material. This also means that almost no projectile kinetic energy goes into to deforming the projectile. From a modelling perspective, this is a good result since the focus is preferably on modelling the target and not the projectile. A near rigid projectile is therefore to be preferred compared to a projectile that deforms considerably.

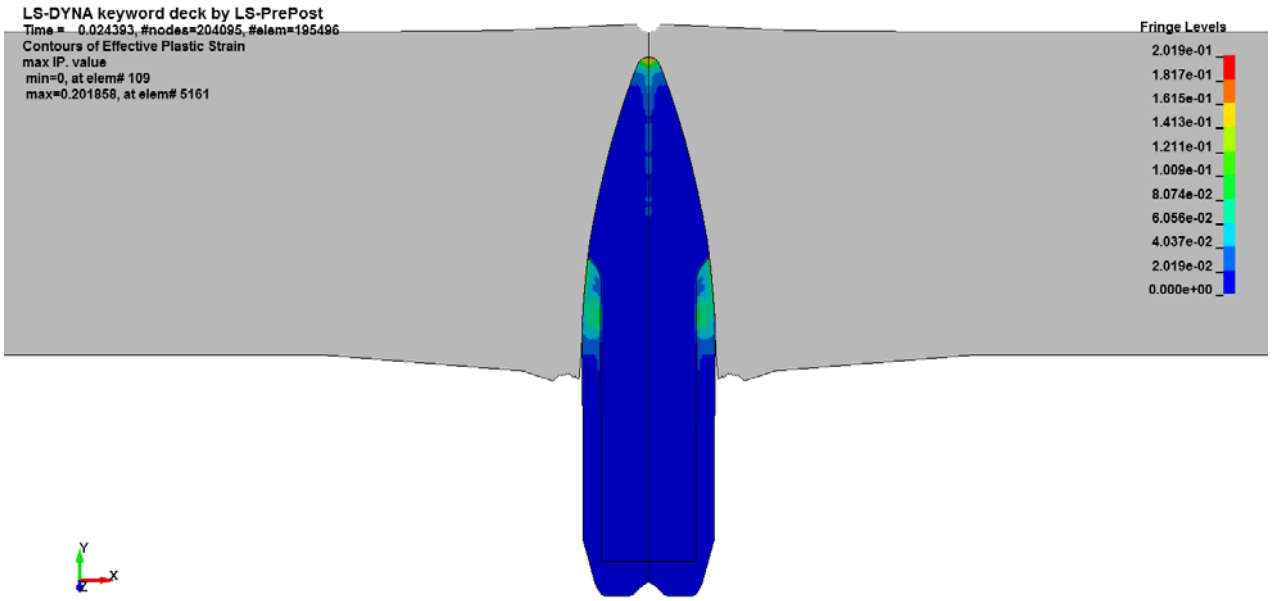

Figure 6. A snapshot of projectile deformation with fringe levels of effective plastic strain.

Sensitivity Study

Different samples of the exact same metal alloy can have very different mechanical properties. These very different mechanical properties are also seen for the specific aluminium alloy in question, where the JC/MJC material parameters found in literature, which are based on mechanical tests, show large variation. To illustrate this variance, the flow stress-strain curve for three different JC/MJC parameter sets of Al7075-T651 are shown in Figure 7.

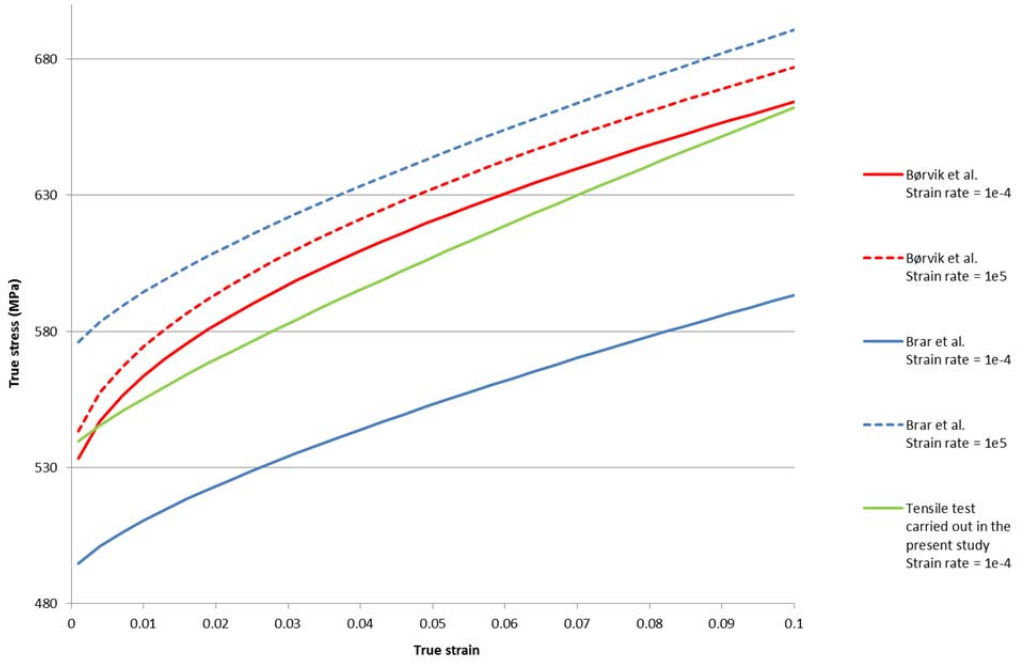

Figure 7. Flow stress-strain curves for three different sets of Johnson-Cook parameters for Al7075-T651, [2], [6]. With Eq. 1 the flow stress-strain curve is established for a quasi-static strain rate ($\dot{\varepsilon}_p$=1e-4 s^{-1}) and a strain rate that can be expected during ballistic testing ($\dot{\varepsilon}_p$=1e5 s^{-1}). Note that temperature is assumed constant and that 10% true strain approximately corresponds to failure strain in a simple tension test. Furthermore only a normal tension test ($\dot{\varepsilon}_p$=1e-4 s^{-1}) is carried out in the present project (green curve) which means that no strain rate dependence is established and therefore the high strain rate curve cannot be computed and plotted.

It is seen that three different parameter sets for the exact same aluminium alloy exhibit a relatively large difference in stress-strain curves. Comparison of the parameter set proposed by Børvik et al. with the one proposed by Brar et al. shows a very big discrepancy in strain-rate sensitivity. Børvik et al. proposes a modified strain rate sensitivity constant C=0.001 which exhibits very small strain rate dependence whereas Brar et al. proposes a high strain-rate sensitivity with constant C_{JC}=0.017. Notice however, that the two strain-rate sensitivity constants cannot be compared directly because the first is the modified strain-rate sensitivity constant and the second is the standard strain-rate sensitivity constant.

The influence of such large parameter variations on the ballistic performance of the target is investigated in the following section. Also the sensitivity to variation in choice of LS-DYNA material model is investigated and lastly a discretization sensitivity analysis is carried out.

Variable Sensitivity Study with LS-OPT®

Parameters of the Johnson-Cook model such as A, B, n, C, m and W_{cr} are determined in material mechanical tests, and as seen in the previous section the parameters have great variance. In sensitivity analyses (or variable screenings) the idea is to analyse the influence of these model variables on the model response. A sensitivity study is carried out by varying the model parameters within a specified range and based on a number of sample calculations model responses can be then be approximated within the full variable range. Sample calculations are carried out on the model with target thickness 20 mm.

The influence of some aluminium MJC variables on the model response (in this case projectile residual velocity) is investigated next. From preliminary sensitivity analyses with realistic variable ranges (i.e. where parameter minimum and maximum values are kept realistic) it was observed that the yield stress/strain hardening term $(A + B\varepsilon_p^n)$, C and m all have significant influence, W_{cr} has minor influence and E, ν and ρ have insignificant influence on the ballistic performance of the target (i.e. residual velocity of projectile). Notice that the influence of yield stress and strain hardening is investigated by varying only the yield stress, A, and keeping the strain hardening parameters B and n constant.

A quadratic polynomial response surface is assumed and the sensitivity analysis parameter setup is seen in Table 3 where the four most influential parameters A, C, m and W_{cr} are investigated.

Parameter	Unit	Starting point	Range
Yield strength A	MPa	520	$470 \leq A \leq 520$
Strain hardening parameter B	MPa	477	$B = 477$
Strain hardening parameter n		0.52	$n = 0.52$
Modified strain rate sensitivity constant C		0.001	$0.001 \leq C \leq 0.0068$
Thermal softening parameter m		1.61	$1 \leq m \leq 1.61$
Critical Cockcroft-Latham parameter W_{cr}	MPa	106	$106 \leq W_{cr} \leq 292$

Table 3. Parameter setup for the sensitivity analysis.

With four model variables a total of 23 sample computations are used to construct the quadratic polynomial response surface. An estimate of the response-surface accuracy is seen in Figure 8. It is seen that the predicted and computed results agree fairly well, and therefore a quadratic polynomial response surface seems to be a fair approximation.

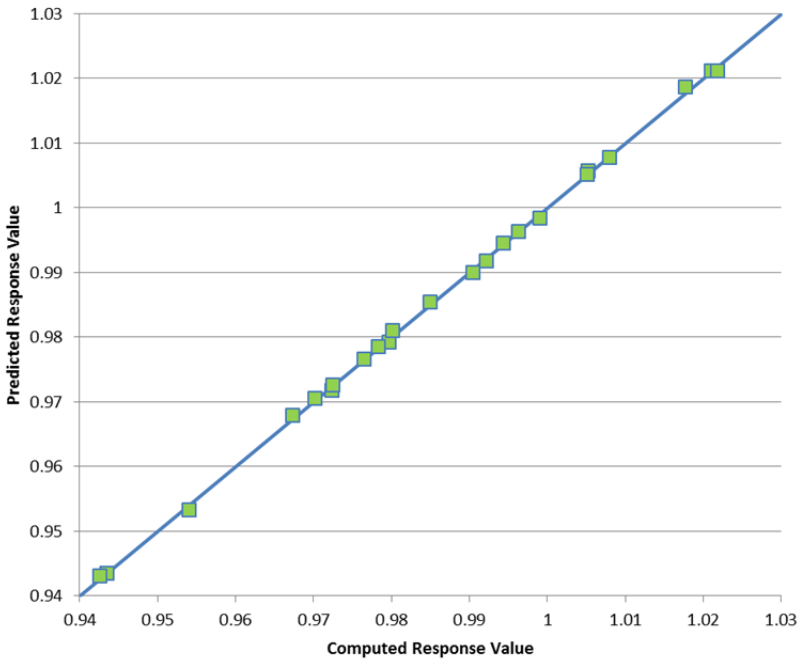

Figure 8. Accuracy of the quadratic polynomial metamodel. Predicted vs. computed normalized residual projectile velocity. The value 1 corresponds to the residual velocity of a model with the starting point values in Table 3.

Figure 9 shows the influence of the four model variables on the projectile velocity. The metamodel predictions of normalized projectile residual-velocity are plotted over the respective parameter ranges in Figure 10.

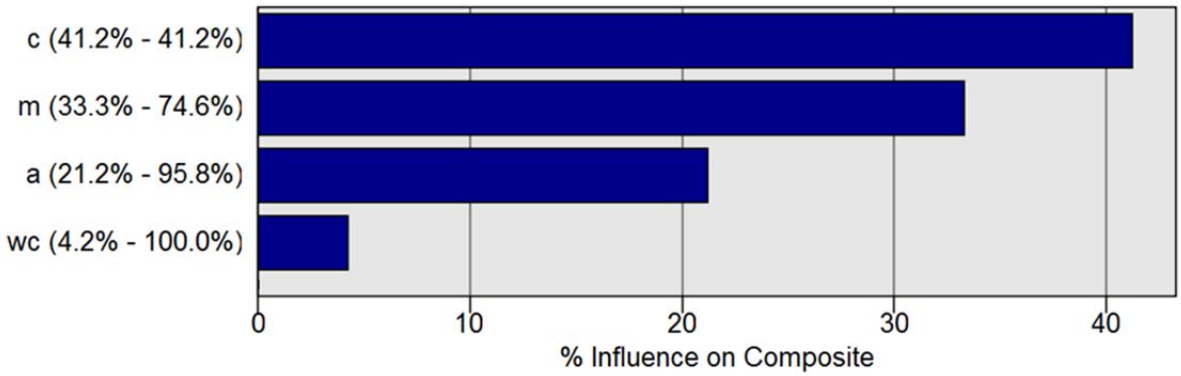

Figure 9. Influence of MJC parameters A, C, m and W_{cr} on the residual velocity of the projectile. Each bar represents the contribution of the variable to the residual velocity of the projectile.

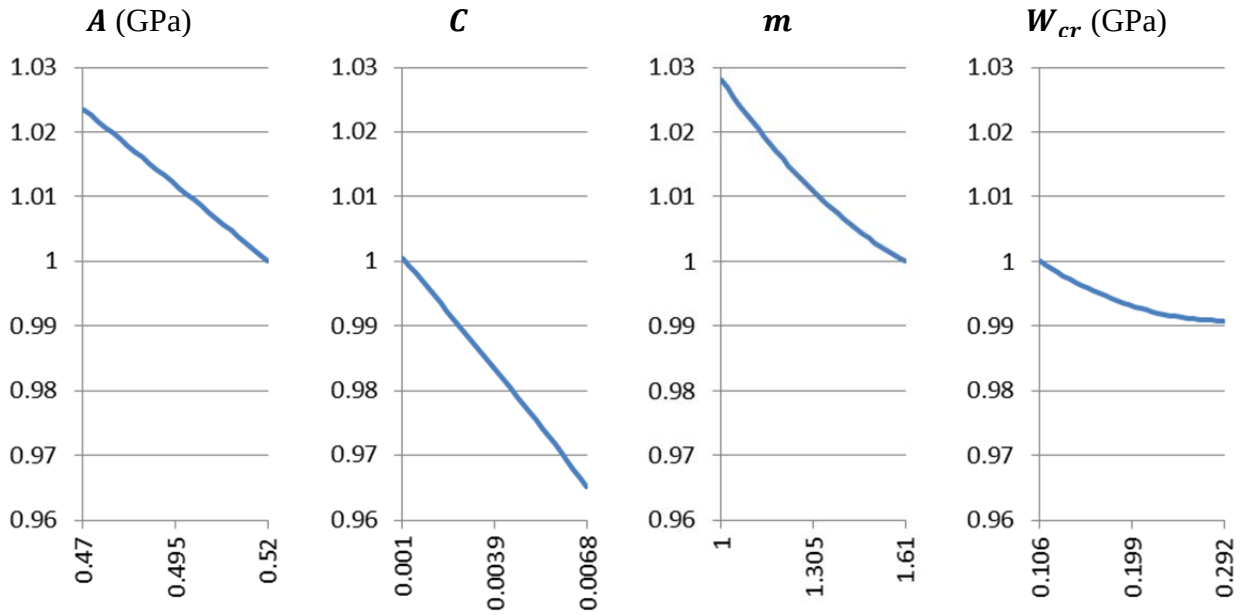

Figure 10. 2-D metamodel surface plots with projectile normalized residual velocity predictions over the respective ranges of A (GPa), C, m and W_{cr} (GPa).

The order of influence on the target ballistic performance is C, m, A and W_{cr}. However, this order depends on the range that the variables are varied within. In this sensitivity analysis, the ranges vary with C + 580%, m – 37%, A – 10% and W_{cr} +175% whereas in a preliminary sensitivity study the ranges were similar with $\pm$15% giving an alternative order of influence: A, m, W_{cr} and C (with the last two having an insignificant influence).

An important observation in Figure 9 is that the influence of W_{cr} on the residual velocity of the projectile is relatively small even though W_{cr} is varied over a large range. W_{cr} is the critical plastic work level where failure is introduced in a finite element model and therefore it can be observed that the CL failure criterion has minor influence on the model result.

It is also interesting to observe that C and m have large influence on the ballistic performance of the target because these parameters are probably amongst the parameters that are most uncertain. The strain rate dependence parameter C for example is typically determined with results from a simple tension test combined with the result of high strain rate test such as the Split-Hopkinson Pressure Bar test. However the Split-Hopkinson Pressure Bar test typically generate material strain rates around 1e3 S^{-1} whereas the model predicts strain rates above 1e6 S^{-1}, i.e. at an elevated strain rate level for which results from the Spilt Hopkinson Pressure bar test cannot be extrapolated.

Looking at the results of the 20 mm plate (see Table 2) the discrepancy between model prediction and ballistic tests can be reduced significantly by introducing a strain rate sensitivity according to Brar et al. instead of Børvik et al., corresponding to a strain rate sensitivity parameter of C=0.0068 instead of C=0.001.

In summation it is concluded that A, C and m all have significant influence on the target ballistic performance and the CL failure model has minor influence on target ballistic performance.

The Johnson-Cook Model vs. Modified Johnson-Cook

In this sensitivity study, MJC for the target material is replaced with JC, i.e. LS-DYNA material type 107 is replaced with type 15. The projectile material models are unchanged and therefore still MJC.

As already noted, JC differs from MJC in terms of strain rate dependence and failure criterion. Furthermore, the Gruneisen equation of state which relates volumetric deformation to pressure is used in the JC model. The strain rate sensitivity constant C_{JC} for the JC is chosen so that the strain rate dependence is similar to that of MJC. The strain-rate dependency of the two models with $C_{JC} = 0.0025$ for JC and $C = 0.001$ for MJC are compared in Figure 11 and exhibit only small differences. In Table 1 the full material model parameter set is displayed.

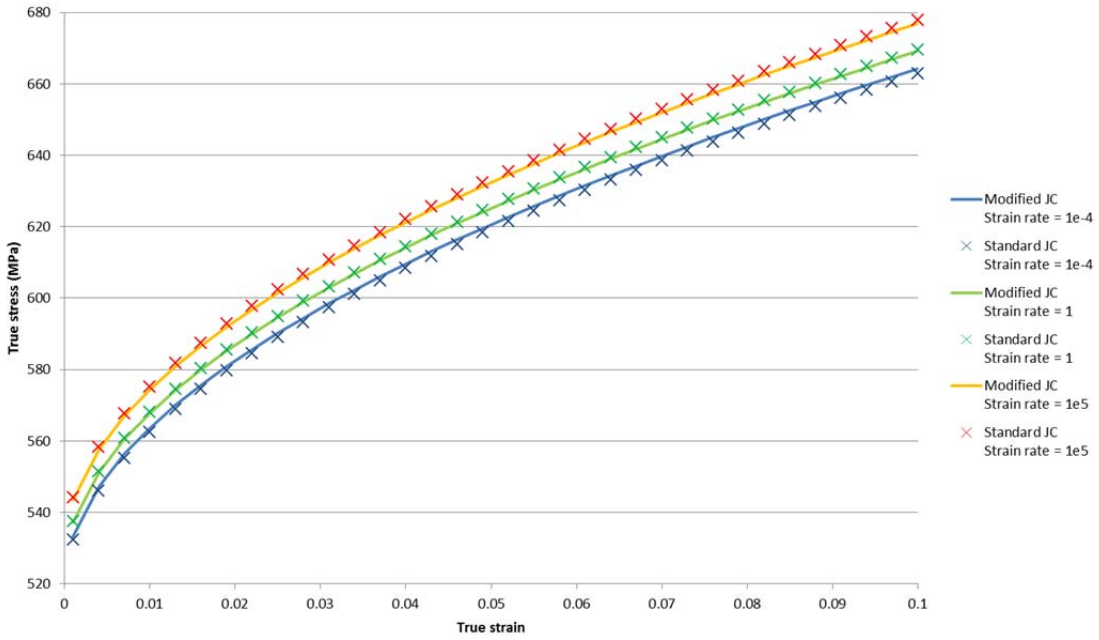

Figure 11. Strain-rate dependence of the standard JC material model ($C_{JC} = 0.0025$) compared with the MJC material model ($C = 0.001$).

Element erosion proved to be an even bigger problem with JC than observed earlier in the MJC. The problem was solved by activating the EROD parameter where element erosion at failure is deactivated and instead the deviatoric stresses are set to zero.

For the 20 mm plate a normalized residual velocity of 1.005 was observed. This means that using the CL failure produces equally as good results as the far more complex JC failure model. This agrees well with the variable sensitivity study where it was observed that the influence of the failure model was small.

In Figure 12 a deformation plot with the JC model is compared with a deformation plot with MJC. It is immediately seen how element erosion is not introduced in the JC model and stress contours have the same overall appearance in both models even though the values are not exactly the same.

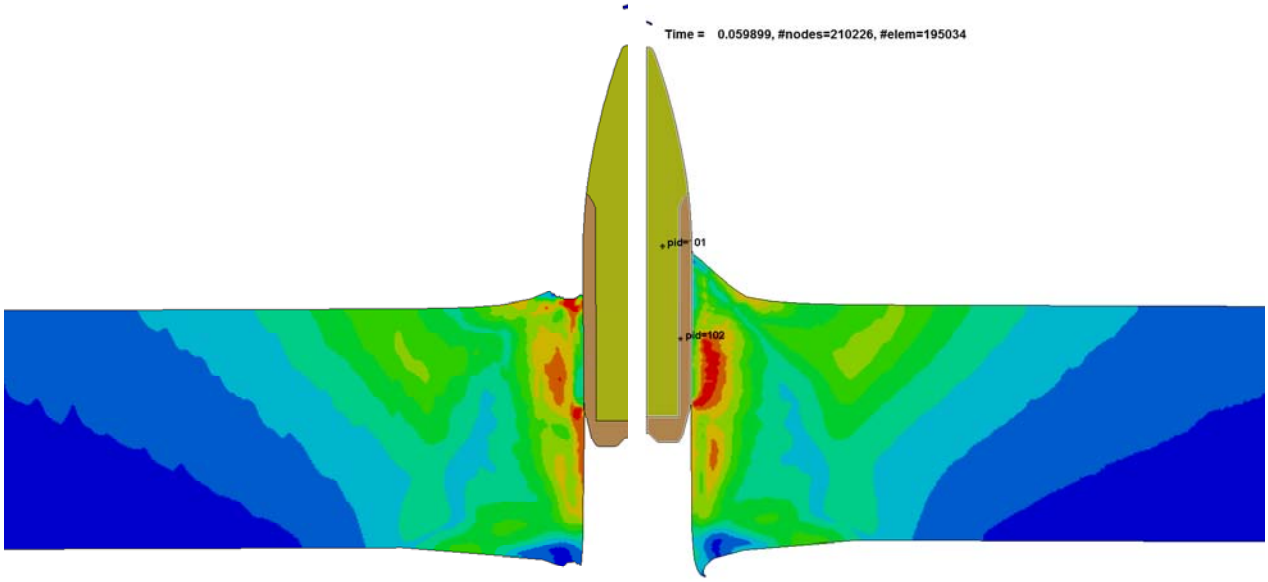

Figure 12. Left: deformation with MJC material model. Right: deformation with JC material model. Fringes show 1st deviatoric stresses.

Element Size Sensitivity

The discretization error has been investigated both in relation to mesh element size and in relation to the time interval between adaptive refinements of the mesh (the ADPFREQ parameter). The discretization error is investigated on the 20 mm model as described in the section: LS-DYNA Model. The result of the discretization error investigation is summarized in Table 4.

Mesh	Element side length	Number of elements	Normalized residual velocity	
			ADPFREQ = 5e-4 msec	ADPFREQ = 2e-4 msec
Coarse	1/4 mm	49,693	0.985	-
Medium	1/6 mm	111,746	1	-
Fine	1/8 mm	198,750	1.005	1

Table 4. Discretization error. For ADPFREQ = 5e-4 msec the adaption frequency is still 2e-4 in a small part of the simulation as described in section: Mesh.

It is seen that the residual velocity difference between the medium and fine mesh is only 0.5%. (for ADPFREQ = 5e-4 msec). It is also seen that increasing the adaption frequency only gives equally minute changes in the residual velocity. It can be concluded that the medium mesh with ADPFREQ = 5e-4 msec is a sufficiently fine discretization, however typically the fine mesh with ADPFREQ = 5e-4 msec have been used.

Conclusion

A LS-DYNA finite element model was successfully developed to simulate perforation of armour-piercing projectiles on hard and thick aluminium alloy targets. The model includes a modified version of the elasto-plastic, strain rate and temperature sensitive Johnson-Cook material model with failure.

Lessons learnt include:

- Validating the predicted residual projectile velocity against live ballistic tests proved inconclusive since the velocity measured in tests had an unknown yet relevant

uncertainty. However, a difference of 5-12% was observed between model and test results which is a difference that according to a parameter sensitivity study can be neutralized with an alternative but still realistic (i.e. available in literature) choice of model parameters for the target material.

- In both the LS-DYNA model and the live ballistic tests a ductile hole enlargement failure mechanism was observed in targets.
- In the aluminium target, yield strength, strain hardening, strain rate sensitivity and temperature sensitivity proved significant in relation to predicting the residual velocity of the projectile.
- When modelling projectile perforation of thick targets with a ductile hole enlargement failure mechanism, the failure model seems to be of minor significance to the residual velocity of the projectile. This also means that using the far simpler Cockcroft and Latham failure criterion as opposed to the Johnson-Cook failure criterion proves to be a perfectly good simplification.
- Implementing an adaptive mesh algorithm for the target proved to be an excellent solution to overcome challenges with large deformations in a Lagrangian finite element model.
- The kinetic energy taken out of the projectile is almost exclusively transferred to the target and converted in to internal energy, i.e. target deformation. That also means that only small projectile deformation is observed in the model.

References

[1] Børvik T, Dey S, Clausen AH. Perforation resistance of five different high-strength steel plates subjected to small-arms projectiles. Int J Impact Eng 2009;36:948-64.

[2] Brar NS, Joshi VS, Harris BW, Constitutive Model Constants for Al7075-T651 and Al7075-T6, CP1195, Shock Compression of Condensed Matter, 2009 American Institute of Physics 978-0-7354-0732-9/09

[3] Dorogoy A, Karp B, Rittel D. A Shear Compression Disk Specimen with Controlled Stress Triaxiality under Quasi-Static Loading. Experimental Mechanics. 05/2012; 51(9):1545-1557. DOI:10.1007/s11340-011-9482-3

[4] ASM Material Data Sheet Aluminum 7075-T6; 7075-T651, http://asm.matweb.com/search/SpecificMaterial.asp?bassnum=MA7075T6

[5] Dey S, Børvik T, Hopperstad OS, Langseth M. On the influence of fracture criterion in projectile impact of steel plates. Computational Materials Science 38 (2006) 176–191

[6] Børvik T, Aunehaugen H, Hopperstad OS, Impact behaviour of the high-strength aluminium alloy AA7075-T651, DYMAT 2009 (2009) 695–701 EDP Sciences, 2009 DOI: 10.1051/dymat/2009098

[7] LS-DYNA Keyword User's Manual, February 2013, Version R7.0, Livermore Software Technology Corporation (LSTC)

[8] Penetration Modeling with LS-DYNA, Seminar notes, November 28-29 2012, Stuttgart